

# Early Glaucoma Involves Both Deep Local, and Shallow Widespread, Retinal Nerve Fiber Damage of the Macular Region

Donald C. Hood,<sup>1,2</sup> Anastasia Slobodnick,<sup>1,3,4</sup> Ali S. Raza,<sup>1,5</sup> Carlos Gustavo de Moraes,<sup>3,6</sup> Christopher C. Teng,<sup>3,7</sup> and Robert Ritch<sup>3,7</sup>

<sup>1</sup>Department of Psychology, Columbia University, New York, New York

<sup>2</sup>Department of Ophthalmology, Columbia University, New York, New York

<sup>3</sup>Einhorn Clinical Research Center, New York Eye and Ear Infirmary, New York, New York

<sup>4</sup>New York University School of Medicine, New York, New York

<sup>5</sup>Department of Neurobiology and Behavior, Columbia University, New York, New York

<sup>6</sup>Department of Ophthalmology, New York University School of Medicine, New York, New York

<sup>7</sup>Department of Ophthalmology, New York Medical College, Valhalla, New York

Correspondence: Donald C. Hood, Department of Psychology, 406 Schermerhorn Hall, 1190 Amsterdam Avenue, MC 5501, Columbia University, New York, NY 10027; dch3@columbia.edu.

Submitted: August 24, 2013

Accepted: December 9, 2013

Citation: Hood DC, Slobodnick A, Raza AS, de Moraes CG, Teng CC, Ritch R. Early glaucoma involves both deep local, and shallow widespread, retinal nerve fiber damage of the macular region. *Invest Ophthalmol Vis Sci*. 2014;55:632–649. DOI:10.1167/iovs.13-13130

**PURPOSE.** To better understand the nature of early glaucomatous damage of the macula by comparing the results from 10-2 visual fields, optical coherence tomography (OCT) macular cube scans, and OCT circumpapillary circle scans.

**METHODS.** One eye of each of 66 glaucoma patients or suspects, with a mean deviation (MD) on the 24-2 visual field (VF) test of better than  $-6$  decibels (dB), was prospectively tested with 10-2 VFs and OCT macular cube and circumpapillary circle scans. Thickness and probability maps of the retinal ganglion cell plus inner plexiform (RGC+) layers were generated. A hemifield was considered abnormal if both the macular RGC+ and the 10-2 probability plots were abnormal (cluster criteria). The thickness plots of the circumpapillary retinal nerve fiber layer (RNFL) were analyzed in the context of a model that predicted the region of the disc associated with macular damage.

**RESULTS.** Twenty-seven hemifields (20 eyes) had abnormal 10-2 and RGC+ probability plots: 7 in upper VF/inferior retina, 6 in lower VF/superior retina, and 7 in both hemifields. Both shallow widespread and deep local thinning of the circumpapillary RNFL were observed. The local defects were more common and closer to fixation in the upper VF/inferior retina as predicted.

**CONCLUSIONS.** A model of glaucomatous damage of the macula predicted the location of both the widespread and local defects in the temporal and inferior disc quadrants. Optical coherence tomography scans of the circumpapillary RNFL and the macular RGC+ layer can aid in the identification of these defects and help in the interpretation of 24-2 and 10-2 VF tests.

**Keywords:** glaucoma, optical coherence tomography, visual fields, optic disc, retinal nerve fiber layer

Over 30% of the retinal ganglion cells (RGCs) are within the macular region,<sup>1</sup> defined here as the central  $\pm 8^\circ$ . While it is clear that early, even initial, glaucomatous damage can involve these RGCs and the macula,<sup>2–13</sup> the nature of this damage is incompletely understood. We recently proposed a model based upon visual field (VF) and optical coherence tomography (OCT) data to explain some of the key aspects of macular damage.<sup>11,12</sup>

According to this model, schematized in Figure 1, the temporal quadrant of the disc contains the axons from RGCs in the gray region, which includes the RGCs of the superior macula and some of the RGCs of the inferior macula. However, most of the inferior RGCs are within the purple borders and their axons project largely to the inferior quadrant of the disc. To relate this structural map to VF defects, we made the commonly accepted assumption that glaucomatous defects are

more likely to occur, and tend to be more severe, in the superior and inferior quadrants of the disc (orange arcs on disc in Fig. 1) than in the temporal quadrant. Thus, the RGCs within the region of the macula shown in gray in Figure 1 are less vulnerable to glaucomatous damage relative to those outside this region. The RGCs just outside this gray region, including most of the lower macula, project to the superior and inferior quadrants and are at greater risk of glaucomatous damage. Of course, the boundaries between more or less vulnerable regions are not as abrupt as shown. Further, there are individual differences in the mapping of RGCs to the optic disc,<sup>14,15</sup> which may in part depend on the degree of elevation of the position of the disc relative to the fovea (see fig. 16 in Ref. 12).

This model<sup>11,12</sup> provides an explanation for why macular defects in the upper VF tend to be more severe and closer to fixation than those in the lower VF.<sup>2,5,7,9,10</sup> Local retinal nerve

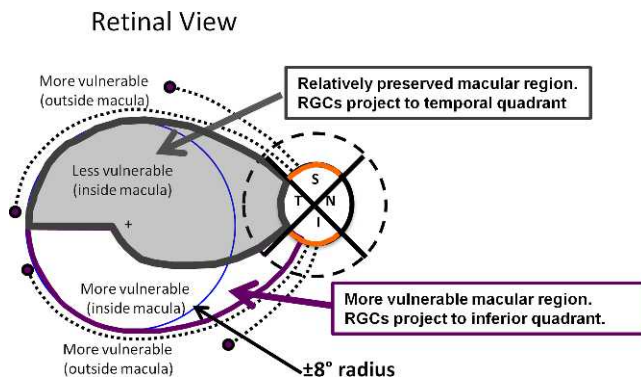


**FIGURE 1.** A model of glaucomatous damage of macula. Modified from Hood DC, Raza AS, de Moraes CG, Liebmann JM, Ritch R. Glaucomatous damage of the macula. *Prog Retin Eye Res.* 2013;32:1-21.<sup>12</sup> Copyright 2013 Elsevier.

fiber layer (RNFL) bundle defects in the temporal part of the inferior quadrant produce focal, arcuate-like VF defects close to fixation in the upper VF. However, the same focal defect in the temporal portion of the superior disc leads to an arcuate-like VF defect of the lower VF that is farther from fixation and largely outside the macula. Consistent with the model, VF arcuate defects occurring largely within the macula (i.e., within  $\pm 8^\circ$ ) are typically seen in the upper VF (inferior retina).<sup>7,9,10,16</sup> In addition, the model predicts the pattern of VF preserved in very advanced glaucoma.<sup>12</sup> However, the model still requires refinement.

While the model was designed to explain the location of relatively local RNFL bundle defects and their associated VF locations, there is evidence that more widespread or diffuse damage of the macula also exists, although there is some debate on this point.<sup>17-23</sup> One purpose of the present study was to test the hypothesis that all macular damage in patients with mild glaucomatous damage is due largely to relatively local RNFL damage at the optic disc. More generally, the purpose here was to better understand the nature of early (mild) glaucomatous damage of the macula, especially its manifestation as damage at the optic disc as seen in circumpapillary RNFL thinning. We excluded eyes with mean deviations (MD) worse than  $-6$  decibels (dB) on 24-2 VFs in order to focus on early damage. In addition, to avoid false positives, eyes selected for OCT RNFL analysis had at least one hemifield that was abnormal on both the 10-2 VF and the OCT macular cube scan.

## METHODS

### Subjects

One eye of 66 open-angle glaucoma suspects and patients was prospectively tested with frequency domain OCT (fdOCT) and 10-2 VFs. Patients were  $\leq 75$  years of age ( $53.8 \pm 15.3$  years), as the control group did not have anyone older than 75. Eyes were included if they had glaucomatous optic neuropathy (GON) on fundus examination and a MD of  $-6$  dB or better on the 24-2 VF (Humphrey VF Analyzer; Carl Zeiss Meditec, Inc., Dublin, CA). Glaucomatous optic neuropathy was defined based on stereophotography evaluation by glaucoma specialists using the following criteria: focal or diffuse neuroretinal rim narrowing, focal or diffuse RNFL loss, or an intereye vertical cup-to-disc ratio asymmetry  $> 0.2$  not explained by differences in disc size. All eyes had open angles as viewed during gonioscopic examination. All patients had fdOCT macular cube and circular disc scans, as well as 10-2 and 24-

2 VFs within 6 months. Twenty-eight (42.4%) of the eyes were classified as high-tension glaucoma (HTG) or were HTG suspects, while 38 (57.6%) were classified as normal-tension glaucoma (NTG) or were NTG suspects. Normal-tension glaucoma was defined based on the presence of all known untreated intraocular pressure measurements lower than 20 mm Hg. Patients were excluded if their cataracts were worse than what we called "early cataracts" as defined during slit-lamp examination. In particular, for inclusion, the scores on the Lens Opacities Classification System III (LOCS III) had to be better than N02, N02, C2, and P2.<sup>24</sup> In addition, eyes had to have a best-corrected visual acuity of 20/40 or better.<sup>25</sup> All eyes with other conditions likely to affect the VF results (e.g., corneal opacity, neurophthalmologic or retinal diseases) were excluded.

Fifty-four healthy eyes of 54 individuals (age  $53.2 \pm 8.1$  years) served as controls for the fdOCT cube scans.<sup>11</sup> They had normal fundus examinations and normal 24-2 VF tests.

### SITA-Standard Protocol

The 10-2 VFs were obtained with the SITA-Standard Automated Perimetry and all met reliability criteria (fixation losses  $\leq 33\%$ , false positives  $\leq 15\%$ , and false negatives  $\leq 20\%$ ). Each hemifield was classified separately and considered abnormal if at least three contiguous test points respecting the horizontal midline were abnormal (at 5%, 5%, 1% or 5%, 2%, 2%) on either total deviation (TD) or pattern deviation (PD) probability plots.

### Frequency Domain OCT

All patients had cube scans of the macula (6 by 6 mm, 128 horizontal B-scans with 512 A-scans each), and all but one had a circumpapillary circle scan (1.7-mm radius, 1024 A-scans with at least 16 overlapping averages [3D-OCT 1000/2000; Topcon Corp., Paramus, NJ]). All scans were oriented along the horizontal meridian, and the cube scans were centered based on the location of the foveal center before analysis. The combined RGC and inner plexiform layers (RGC+) of the OCT scans were segmented using a computer-assisted manual segmentation technique.<sup>26,27</sup> Figure 2A illustrates the segmentation of the center scan from a macular cube scan.

**RGC+ Thickness and Probability Maps.** For each eye, RGC+ thickness maps were produced from the segmented OCT cube scans (Fig. 2B, upper left). Probability maps were obtained from the RGC+ thickness maps after a point-by-point comparison to control values (Fig. 2B, lower panel).<sup>27</sup> Probability values were obtained by fitting a Gaussian distribution to the control data, which assumes a normal distribution.

**OCT RGC+ Classification.** In order to classify the macular scans and 10-2 VFs in a similar manner, RGC+ thickness maps (Fig. 2B, left) were downsampled into an 8 by 8 grid (64 locations) and coded for probability based upon control data (Fig. 2B, right). A hemifield was considered abnormal if at least three contiguous abnormal squares respecting the horizontal midline were abnormal (at 2%, 2%, 1%). By this criterion, 5 of the 108 hemifields of the control eyes were abnormal, yielding a false-positive rate of 4.6%.

**Classification Scheme.** To help ensure we are dealing with real defects, that is, to avoid false positives, only the hemifields abnormal on both the VF and OCT RGC+ maps were included in subsequent analyses. This resulted in 27 abnormal hemifields and 20 eyes. We divided the 20 eyes into three groups (Upper, Lower, Both) depending upon whether the upper VF (inferior retina), lower VF (superior retina), or both hemifields were abnormal using the cluster criteria described above.

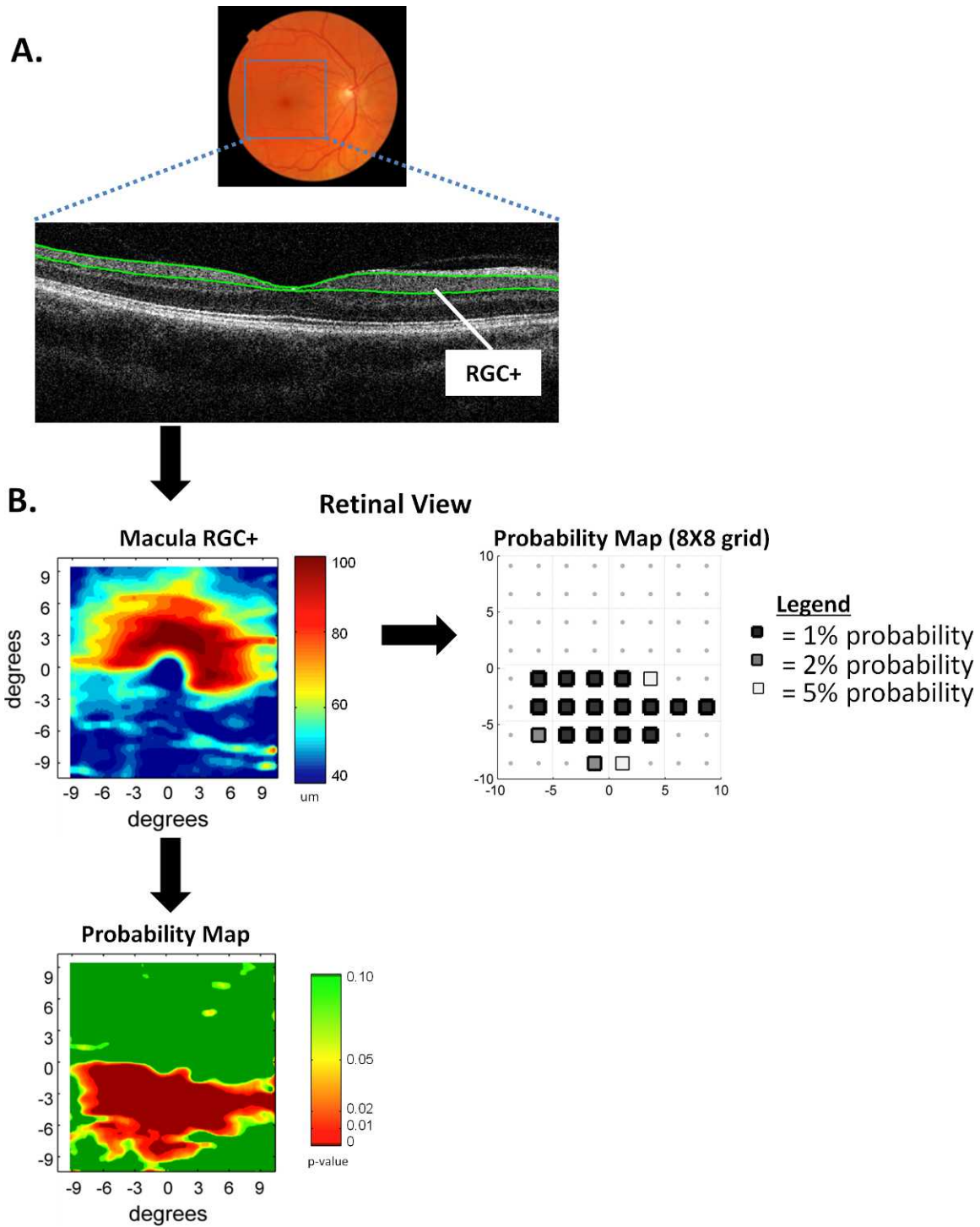


**FIGURE 2.** The fdOCT RGC+ data from a patient (P1). **(A)** A single OCT B-scan along the horizontal meridian from a macular cube scan. The retinal ganglion cell plus inner plexiform (RGC+) layer is shown. **(B)** The macular RGC+ thickness map for each eye from the segmented cube scan. A continuous probability map (*lower*) and an 8 × 8 grid probability plot (*right*) were derived by comparing local thickness to that of the healthy control group.

**Circumpapillary OCT Analyses.** The circumpapillary RNFL thickness was obtained after correction of the segmented RNFL on the circle scan (upper panel in Fig. 3A) and plotted as the black curve in the lower panel of Figure 3A. Notice that the temporal quadrant is shown in the center. That is, this is a Nasal-Superior-Temporal-Inferior-Nasal (NSTIN) plot, not a Temporal-Superior-Nasal-Inferior-Temporal (TSNIT) plot.

**Prediction From the Model**

To relate the RNFL plots in Figure 3A (black curve) to the model, we needed to specify the boundaries of the macular RGCs' input to the disc. The boundaries chosen are shown in Figure 3C. The upper boundary was set at 45°, the boundary of the temporal and superior quadrants of the disc. The boundary

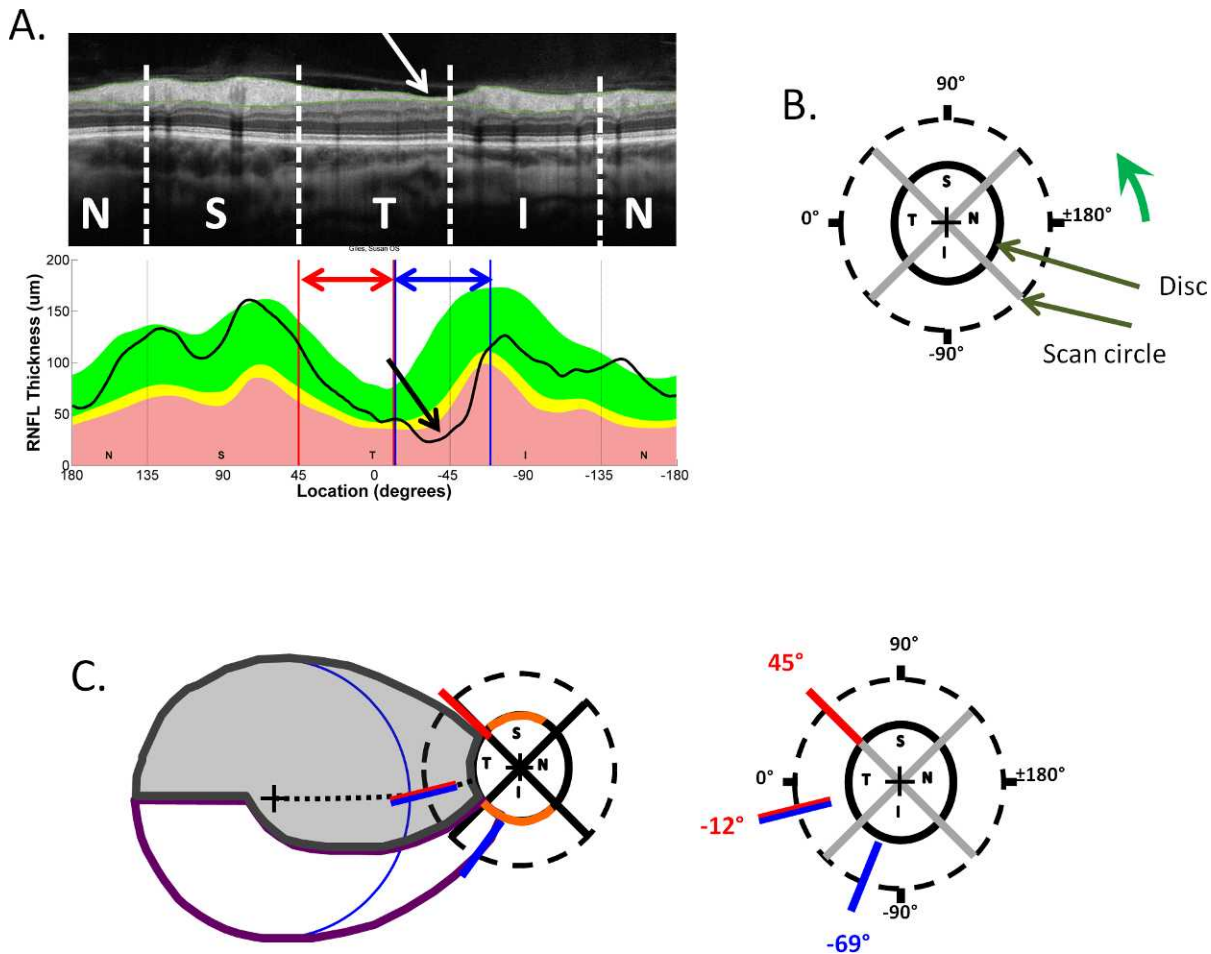


FIGURE 3. (A) A circumpapillary circle scan from P1 with the retinal nerve fiber layer (RNFL) segmented (*above*) and, *below*, the RNFL thickness profile along with the confidence regions for 5% (*yellow*) and 1% (*red*). (B) A schematic of the optic disc showing the orientation and location of the circle scan. (C) The schematic model (*left*) with the regions associated with each hemifield within the central  $\pm 8^\circ$  along with (*right*) the schematic of the disc showing the regions the model associates with the superior retina (*red*) and inferior retina (*blue*).

between the superior and inferior macular region was set at  $-12^\circ$  based upon our tracing of RNFL bundles (Fig. 15 in Ref. 12). Finally, the inferior border was set at  $69^\circ$  to include the region, called the macular vulnerability zone (MVZ),<sup>11,12</sup> associated with macular defects of the upper VF and to have the same width ( $57^\circ$ ) as the superior region at the disc. As mentioned above, individuals vary<sup>12,14,15</sup> and boundaries are not sharp. In any case, the main conclusions here do not depend upon these exact values.

The boundaries of the model are superimposed on the RNFL plots as in Figure 3A. Thus, according to the model, for upper macular ( $\pm 8^\circ$ ) VF defects, there should be abnormal thinning within the region bordered by the blue vertical lines and shown as the horizontal blue line with arrows. Likewise, for lower macular ( $\pm 8^\circ$ ) VF defects, we should see abnormal thinning within the region bordered by the red vertical lines and shown as the horizontal red line with arrows.

### RESULTS

In 20 of the 66 eyes, at least one hemifield was abnormal on both OCT and 10-2 VF tests. Both hemifields were abnormal in 7 of these 20 eyes, while only the upper VF (inferior retina) was abnormal in 7 eyes and only the lower VF (superior retina) in 6 eyes for a total of 27 abnormal hemifields. The Table contains some key information about these 20 eyes.

### Group Data

Figure 4 shows average results for the three groups with abnormalities only in the upper, only in the lower, or in both hemifields. Results are presented as right eyes. The hemifield of interest is enclosed within a colored rectangle, blue for upper VF/inferior retina and red for lower VF/superior retina.

The leftmost panels show the average 10-2 results (field view) as TD (dB) values in pseudocolor. The points of the 10-2 were morphed to take the displacement of the RGCs near the fovea into consideration, as previously described.<sup>10,27,28</sup> The pattern of defects differed for the Upper and Lower VF groups. The average upper VF defects (Fig. 4A) were deeper (i.e., more negative TD values) and closer to fixation than the lower VF defects (Fig. 4B). The eyes with both hemifields classified as abnormal (Fig. 4C) showed less deep VF defects in the upper VF than did the Upper group.

The middle panels of Figure 4 show the RGC+ thickness maps (see Fig. 2B) in retinal view. The RGC+ results are in agreement with the 10-2 VF results. The RGC+ thinning in the lower retina of the Upper group is more extreme, and closer to fixation than the RGC+ thinning in the upper retina of the Lower or Both groups.

The results from the circumpapillary scans are of particular interest for this study. The rightmost panels of Figure 4 show the average circumpapillary RNFL plot. The Upper VF group

TABLE. Basic Information About the 20 Eyes With Abnormal 10-2 Visual Fields and OCT Macular RGC+ Scans

Group	Patient	Age	Eye	DX	HT/NT	VA	24-2 MD	10-2 MD	Mean TD Upper	Mean TD Lower
Upper VF	P1	48	OS	POAG	HTG	20/25	-2.7	-8.23	-16.38	-1.88
	P2	74	OS	POAG	NTG	20/20	-1.7	-5.84	-13.23	-0.97
	P3	78	OD	POAG	NTG	20/20	-3.5	-5.94	-10.38	-2.18
	P4	56	OS	POAG	NTG	20/20	-1.3	-1.69	-4.35	0.70
	P5	52	OD	POAG	NTG	20/20	-0.5	-1.27	-2.44	-0.41
	P6	66	OD	XFG	HTG	20/15	-1.4	-0.61	-2.35	0.97
	P7	47	OD	PG	HTG	20/20	-0.9	-1.35	-1.35	-1.35
Average		60.1					-1.7	-3.56	-7.21	-0.73
Lower VF	P8	72	OD	POAG	HTG	20/40	-3.5	-3.83	-2.79	-5.06
	P9	62	OS	POAG	NTG	20/25	-1.6	-2.88	-0.26	-4.85
	P10	70	OS	GS	NTG	20/25	-3.2	-1.84	-1.68	-2.00
	P11	67	OS	POAG	NTG	20/25	0.1	-1.70	-1.18	-1.56
	P12	60	OS	GS	NTG	20/20	0	-0.58	0.29	-1.44
	P13	67	OS	XFG	HTG	20/20	-1.4	-0.51	-0.32	-0.68
Average		66.3					-1.6	-1.89	-0.99	-2.6
Both	P14	55	OS	JOAG	HTG	20/20	-5	-6.82	-10.44	-3.71
	P15	66	OD	PG	HTG	20/20	-4.7	-6.01	-6.97	-5.20
	P16	74	OS	XFG	HTG	20/50	-3.7	-4.15	-4.47	-3.97
	P17	68	OS	POAG	HTG	20/20	-4.5	-3.66	-3.29	-4.21
	P18	67	OD	POAG	NTG	20/20	-3.8	-3.13	-3.12	-3.15
	P19	57	OD	PG	HTG	20/20	-3.6	-2.82	-3.06	-2.24
	P20	70	OD	POAG	HTG	20/20	-1.1	-2.24	-1.91	-2.47
Average		65.3					-3.8	-4.12	-4.75	-3.56

DX, diagnosis; HT, high tension; NT, normal tension; VA, visual acuity; POAG, primary open angle glaucoma; XFG, exfoliative glaucoma; PG, pigmentary glaucoma; GS, glaucoma suspect; JOAG, juvenile open-angle glaucoma.

shows a relatively local RNFL defect with a thinning within the region between the blue vertical lines as predicted by the model (Figs. 1, 3). The peak of this thinning is near the border of the temporal and inferior quadrants of the disc. On the other hand, the average RNFL for the eyes with both hemifields abnormal shows a more widespread and shallower thinning throughout the region between the red and blue vertical lines, that is, the region associated with the macula by the model. The RNFL thinning in the Lower VF group is subtler. However, the RNFL thickness fell below the 95% confidence limit (yellow region) in the region around the border of the temporal and superior quadrants of the disc. This is the region expected from the model to be associated with the defects seen on the 10-2 VF and RGC+ map for the Lower VF group.

### Individual Data

The data for each of the 20 eyes are presented in Figures 5 through 7. All results are presented as if from right eyes. The format for each eye in Figures 5 through 7 is the same. The upper row contains the TD probability plot (left) and the TD values (right) for the 10-2 VF test, both in field view. For the latter, the locations of the test points were morphed as above.<sup>10,27,28</sup> The middle two panels are the total thickness and probability maps for the RGC+ layer presented in retinal view. The bottom row has the RNFL thickness (black curve) for the circumpapillary scan along with the confidence limits for the healthy controls from the OCT machine.

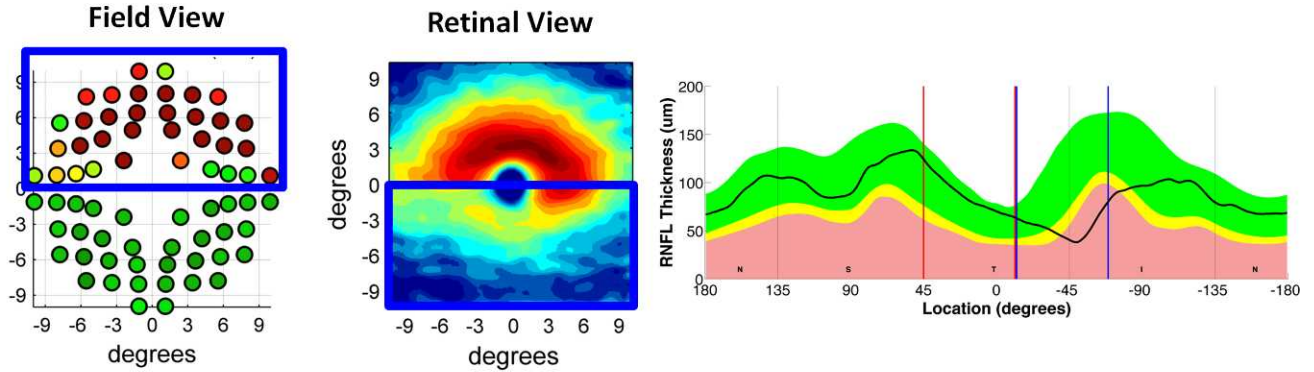
**Upper VF Abnormal.** Figure 5 contains the results for the eyes in which only the Upper VF (inferior retina) was abnormal; they are ordered by mean TD in the upper hemifield of the 10-2 VF test from largest (patient [P1]: -16.4 dB) to smallest (P7: -1.4 dB) loss. The blue rectangle indicates the region of interest. The pattern of results was extremely similar in 6 of these 7 eyes (P1-P6) and similar to the overall average

for this group in Figure 4A. First, the upper hemifield of the 10-2 VF (top panels in Fig. 5 for each eye) showed relatively severe local damage with regions of loss of -8 dB or more. In fact, in P1 through P4 the local loss exceeded -27 dB. Second, the RGC+ thickness and probability maps (the panels on second row) showed damage largely, if not entirely, in the inferior retina (upper VF). Furthermore, the RGC+ thinning was extreme in at least part of the macular region, as seen on the thickness and probability maps.

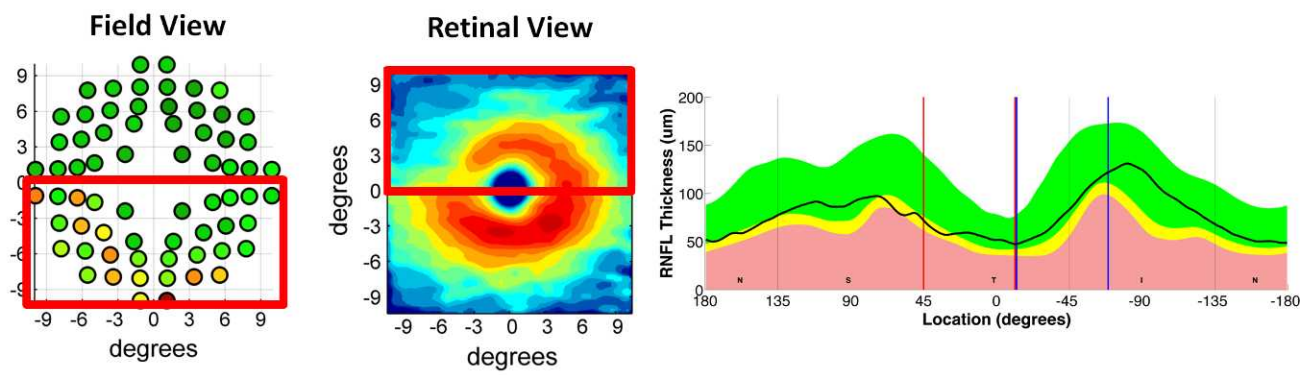
The RNFL thickness plots (third row) for P1 to P6 showed local thinning in the region predicted by the model (i.e., between the blue vertical lines). In fact, this thinning was relatively extreme (deep), extending well into the red (1%) region on the RNFL plot. On the OCT scans, it appears as a nearly complete thinning of the RNFL in all 6 of these eyes. This region of extreme thinning is illustrated in the case of P1 in Figure 3A, where it is marked with white and black arrows. Two more examples, P2 and P4, are shown in Figures 8A and 8B. The point of maximum thinning tended to be close to the border of the temporal (T) and inferior (I) quadrants in these 6 eyes. Further, these defects were relatively local; the RNFL thickness was in the normal range over portions of the temporal region of the disc associated with the macula. We will call these "deep local defects" of the macular RNFL.

Patient 7 presented with a very different pattern of results. In particular, the VF and OCT results suggest a milder and more widespread loss in both upper and lower hemifields. The average TD of the upper VF was only -1.35 dB and was the same as that of the lower VF. Further, the probability and thickness maps show changes of approximately the same degree in both hemispheres. Finally, the RNFL is borderline abnormal (yellow zone) throughout the 114° region (from +45° to -69° in Fig. 3C) predicted by the model, as well as beyond the border of the model in the inferior quadrant. It is possible that this eye is a false positive; that is, it does not have

**A. Upper VF Abnormal (n=7)**



**B. Lower VF Abnormal (n=6)**



**C. Both Upper and Lower VF Abnormal (n=7)**

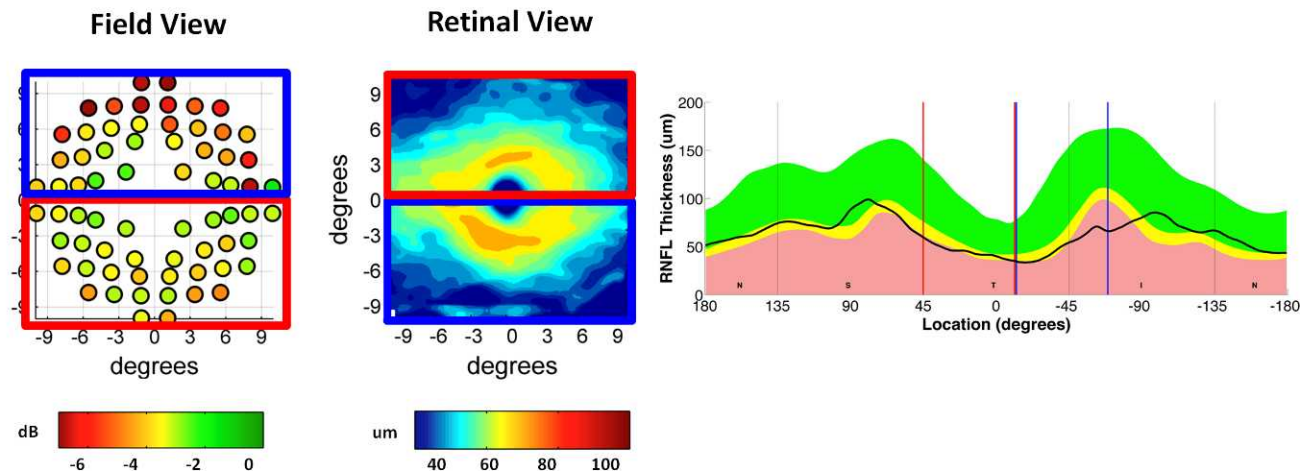
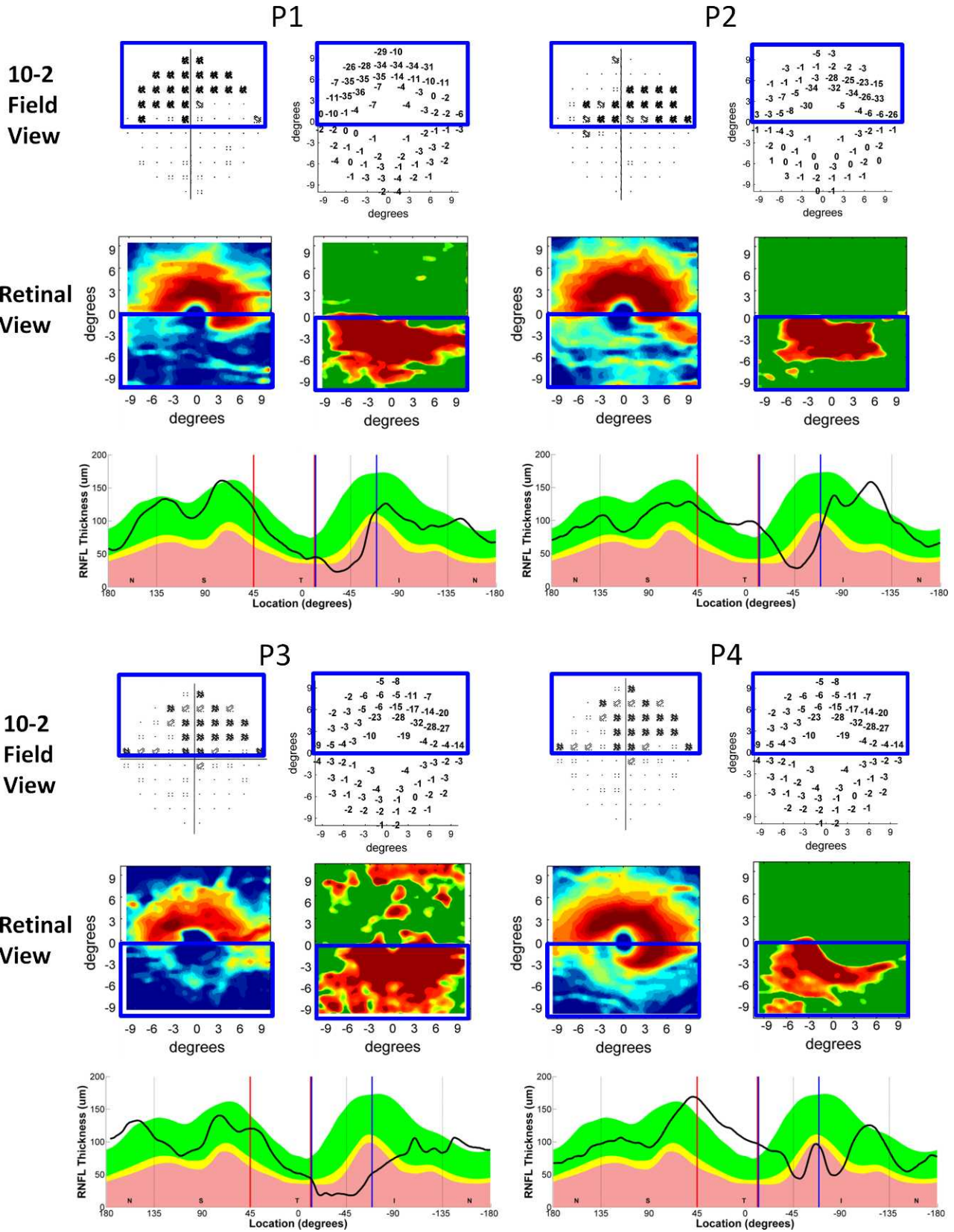
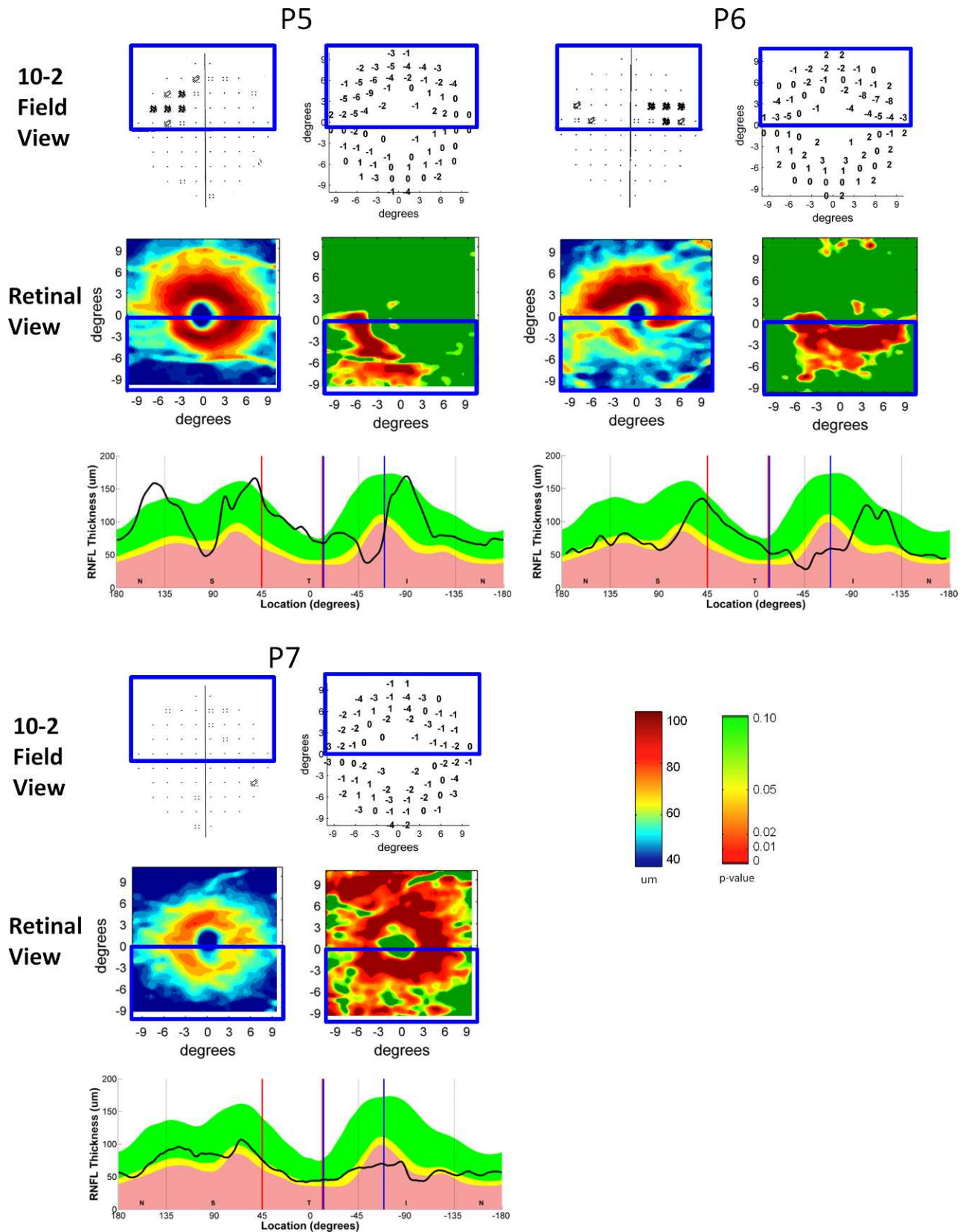


FIGURE 4. Averaged data for eyes with abnormal 10-2 VF and fdOCT RGC+ only in the upper VF/inferior retina (A), only in the lower VF/superior retina (B), or in both upper and lower VFs/retina (C). In each case the average 10-2 total deviation plot (morphed and in pseudocolor), the RGC+ thickness map, and the circumpapillary RNFL thickness plot are shown.

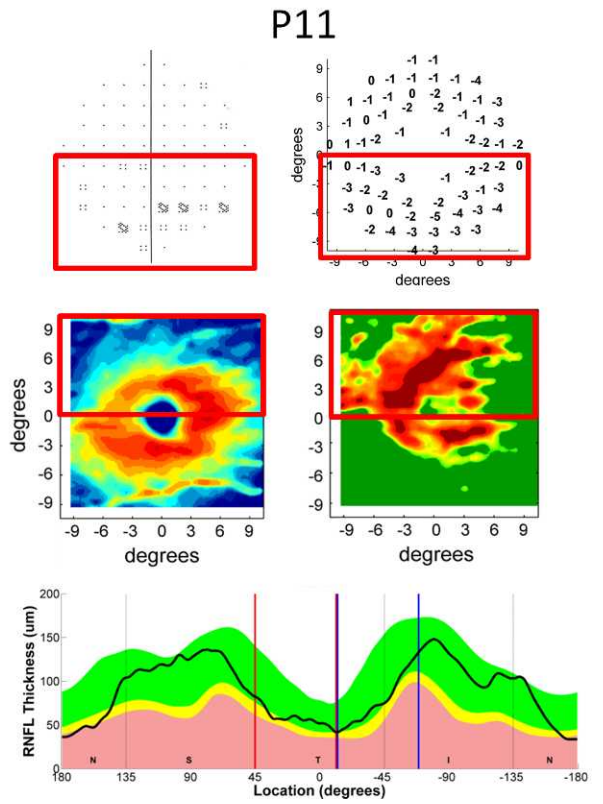
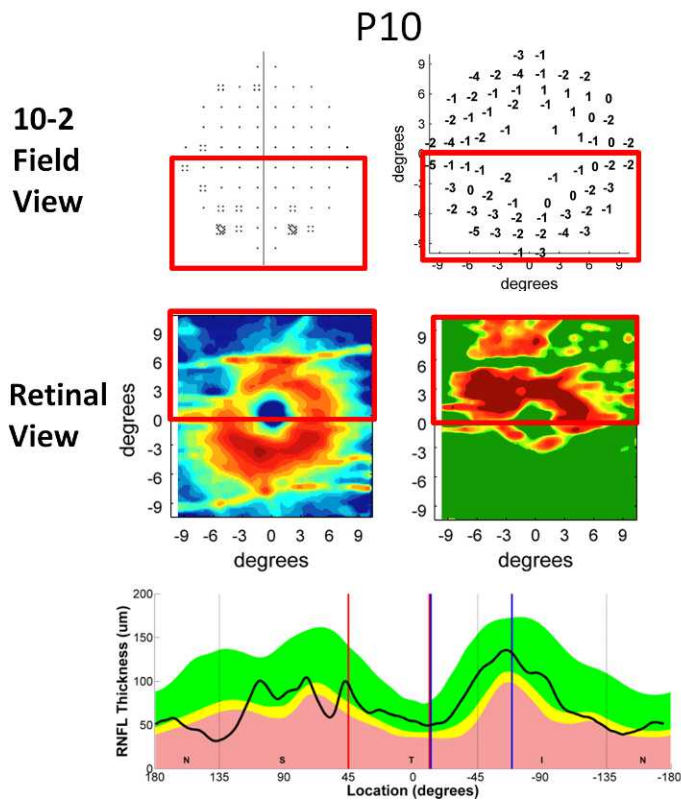
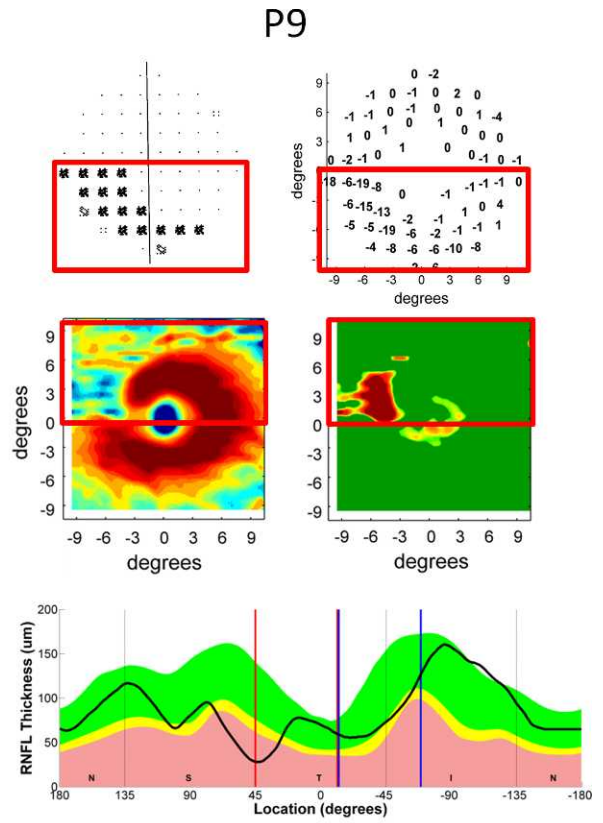
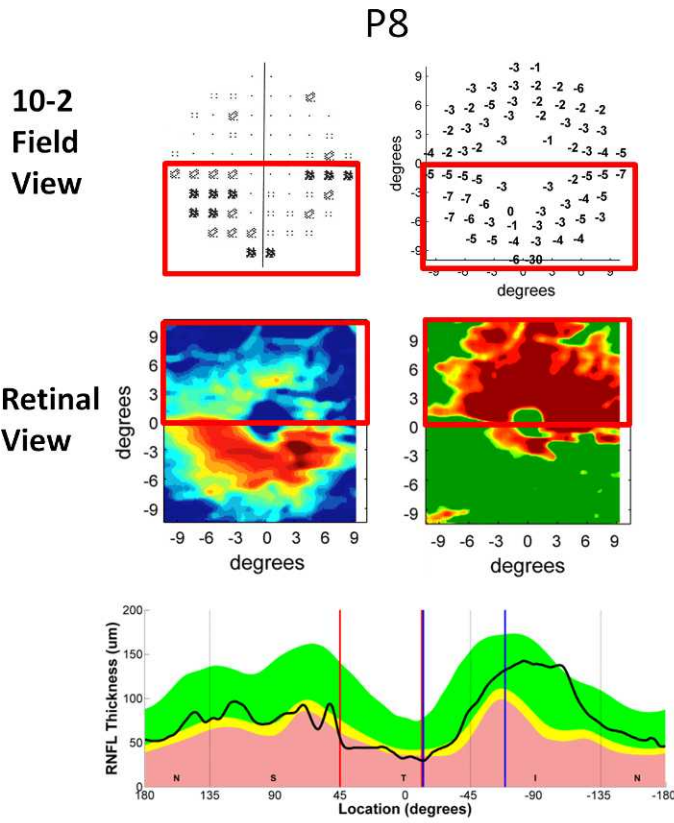
glaucomatous damage. However, we think it more likely that damage in the lower VF/superior retina was missed on the VF, but is seen clearly on the RGC+ maps, which show clear damage to both hemispheres. In fact, as will be seen below, the pattern of RNFL thinning is very similar to that seen for the Both group, where both hemifields were categorized as abnormal.

**Lower VF Abnormal.** Figure 6 contains the results for the eyes in which only the Lower VF was abnormal; they are ordered by the mean of the 10-2 TD values in the lower hemifield from largest (P8: -5.1 dB) to smallest (P13: -0.7 dB) loss. The red rectangle indicates the region of interest. Of the 6 eyes, only P9 showed deep local damage similar to that seen in P1 to P6 of the Upper VF group. In particular, P9's 10-2 VF





**FIGURE 5.** Upper group (P1-P7). Individual results for 7 patients whose OCT RGC+ maps and 10-2 VF tests showed abnormalities in the inferior retina/ upper VF. For each eye, the *upper row* shows the probability plot (*left*) and total deviation (TD) values for the 10-2 VF. The *second row* contains the RGC+ thickness (*left*) and probability (*right*) maps. The color code for these plots is shown at the *bottom* of the figure. The *bottom row* is the circumpapillary RNFL thickness (*black*) with vertical lines indicating the region of the scan associated with the macula according to the model in Figure 2. The *color regions* indicate the confidence limits from machine controls (*green*: within 95%; *yellow*: between 95% and 99%; *red*: beyond 99%). All eyes are presented as right eyes; OCT data are in retinal view and VF data in field view. The *blue rectangle* shows the region of interest.



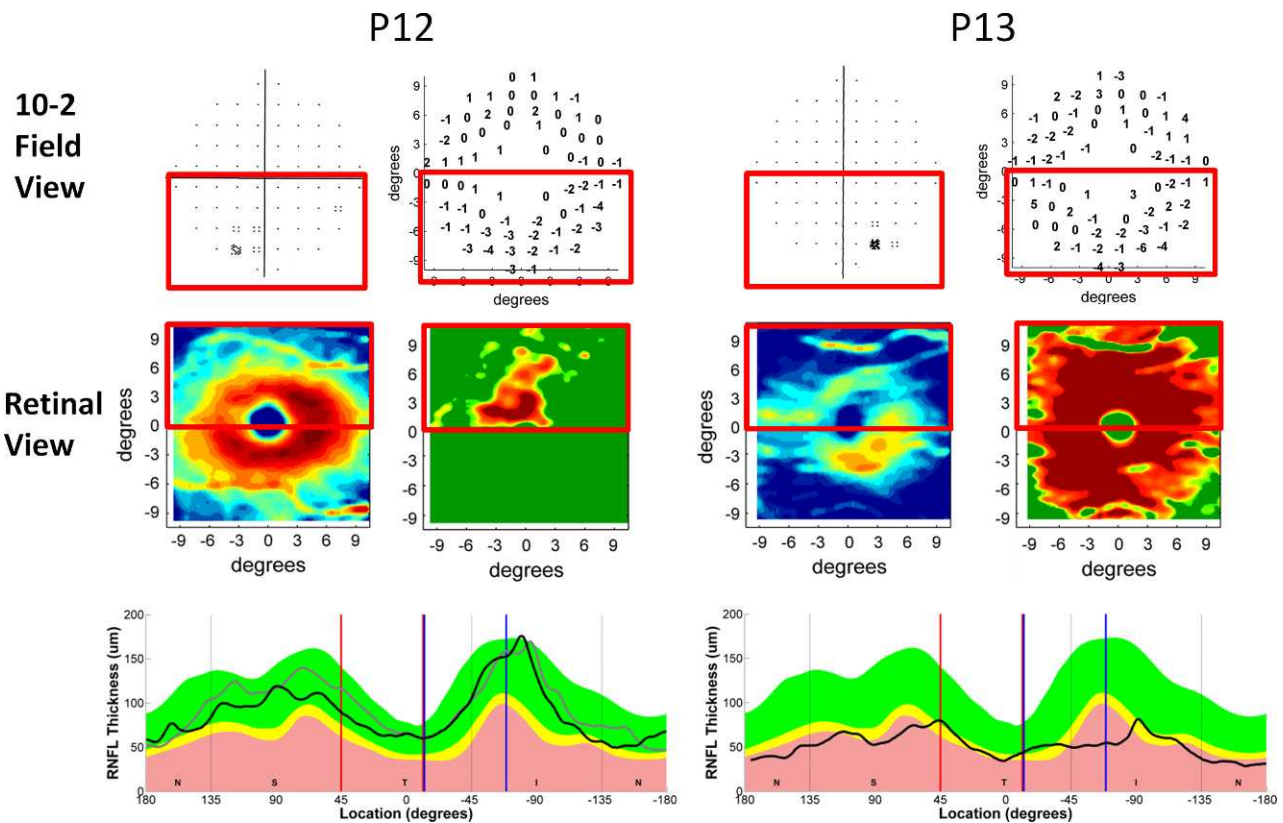


FIGURE 6. Lower group (P8-P13). Same as in Figure 5 except for 6 patients whose OCT RGC+ maps and 10-2 VF tests showed abnormalities in the superior retina/lower VF. The *red rectangle* shows the region of interest.

showed local TD values as large as  $-19$  dB, and the RGC+ maps indicated a deep loss of the RGC layer largely in one hemifield. The RNFL plot has a marked thinning on the border of the temporal and superior quadrants, which can be seen in Figure 8C (white arrow).

The pattern of results in the other 5 eyes was markedly different and was more similar to the average results for this group in Figure 4B. First, the VF defects were milder. The mean TD for the lower hemifield of all 6 eyes was  $-2.6$  dB compared to  $-7.2$  dB for the seven upper hemifields in the Upper group (Table). The defects were also shallower than those in the Upper group. Only one point in all five lower VFs was less than  $-7$  dB. Second, while the RGC+ thickness and probability maps showed clear thinning in the superior retina, in general, this thinning was not as extreme as that seen in Figure 5 for the affected hemifield of the Upper group.

Third, while the RNFL thickness plots (third row) showed local thinning in the region predicted by the model (i.e., between the red vertical lines), the RNFL thinning in this region was less obvious than for the Upper group. Although it involved the red (1%) region in the case of P8 and P9, it was borderline abnormal in P11 and P13 and in the normal range in P10 and P12. However, the VF and OCT data taken together suggest shallow damage in these 5 eyes. This damage is apparent on the RGC+ maps, but can be subtle, or even missed, on the circumpapillary RNFL plot. Further evidence that the RNFL plot may miss subtle damage in the temporal quadrant can be seen in the case of P12 in Figure 6, where the gray curve is the RNFL thickness for the patient's other eye, with better vision. This other eye had a better VF and a clearly thicker RNFL in the macular region between the red vertical lines. This supports the view that the temporal

RNFL thickness of the affected eye of P12 had been diminished, but the thinning did not fall below the normal limits. In addition, P9, P10, and P13 had multifocal visual evoked potential (mfVEP) tests that corroborated the macular damage suggested by the 10-2 and RGC+ maps. In the case of P13, the mfVEP showed both upper and lower macular abnormalities. The mfVEP results, together with the RGC+ map and RNFL plot, suggest that this eye had damage throughout the macula region, like the eyes in the Both group discussed next.

**Both Hemifields Abnormal.** Figure 7 contains the results for the eyes in the Both hemifield group ordered by the overall mean TD loss (MD) from largest (P14:  $-6.8$  dB) to smallest (P20:  $-2.2$  dB). Except for P14, the mean TD values of the upper and lower 10-2 VFs were within 2 dB of each other (Table). The mean TD values of the upper and lower VFs were  $-4.8$  dB (upper) versus  $-3.6$  dB (lower) with P14 and  $-3.8$  dB (upper) and  $-3.6$  dB (lower) without P14. Only the upper 10-2 VF of P14 showed the kind of deep 10-2 defect seen in the upper 10-2 VF of P1 to P4 and in the lower VF of P9. In general, the 10-2 VFs and the RGC+ maps argue for shallower and more widespread damage of the entire macular region than seen in the Upper group of eyes.

The RNFL plots are in agreement. All 7 eyes show an abnormal thinning of the RNFL throughout the  $114^\circ$  region associated with the macula according to the model, that is, throughout the regions within the blue and red vertical lines. The abnormal RNFL thinning extended beyond this region into the inferior and/or superior quadrants. The thinning outside the macula region ranged from relatively deep (red region) to borderline (border of yellow and green regions). In Figure 8, P17 (Fig. 8D) is an example of the former and





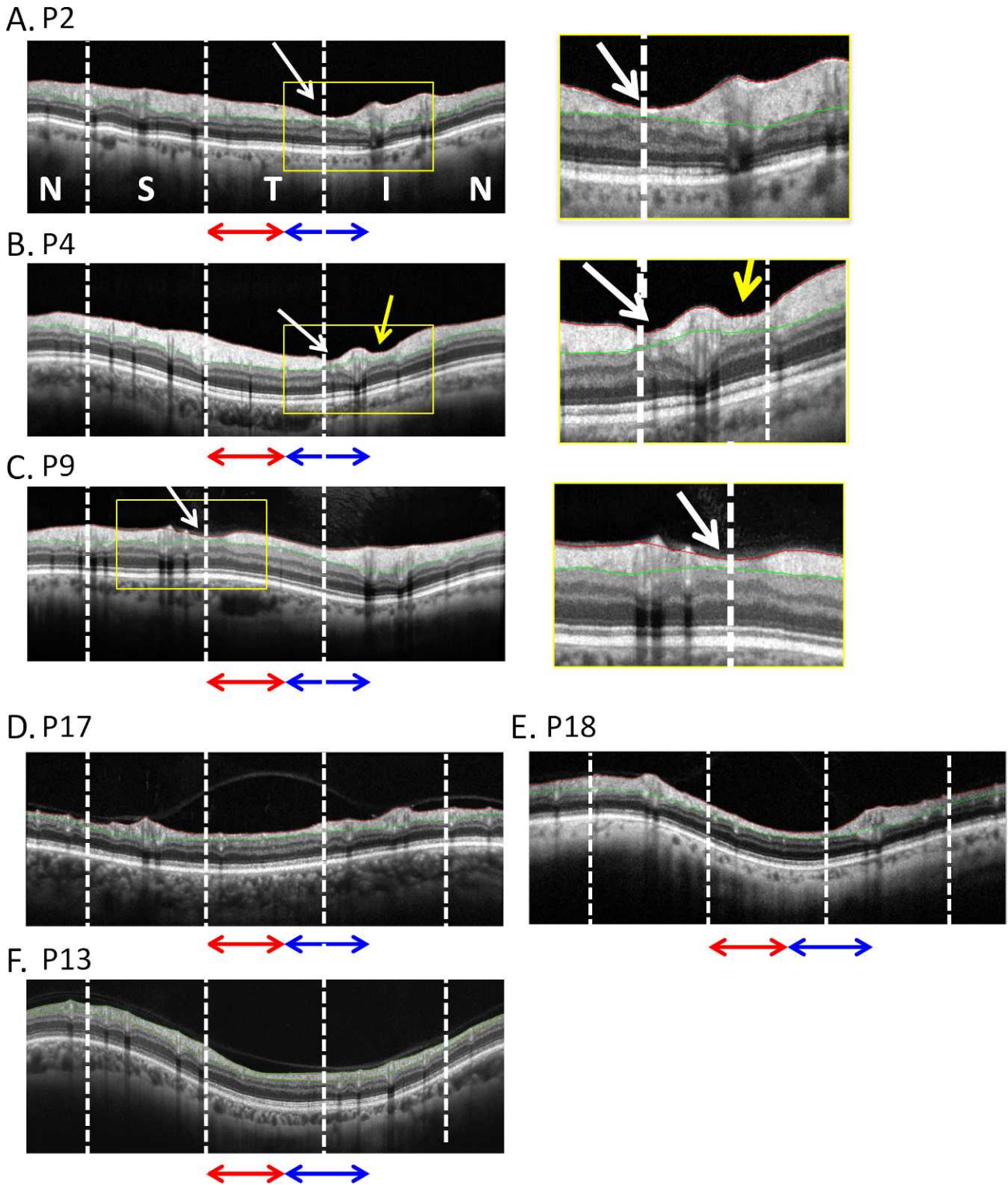


FIGURE 8. (A) Circumpapillary OCT scans for P2. The dashed white lines show the boundaries of the quadrants, the red and blue arrows the regions associated with the model in Figure 2; the white and yellow arrows point to deep local thinning, and the yellow rectangle is the region expanded in the right panel. (B, C) Same as in (A) for P4 and P9. (D–F) Same as in (A) without expanded region for P17, P19, and P13.

P18 (Fig. 8E) of the latter. In general, the RNFL can be said to exhibit widespread shallow damage in the portion of the disc associated with the macula, although there were inferior RNFL regions of relatively deep damage in P14, P17, and P19. However, none of the seven inferior macular regions

showed a deep defect at the border of the temporal and inferior quadrants as seen in the Upper group. That is, the damage in these eyes cannot be described simply as a combination of the damage seen in the Upper and Lower groups.

## Macular Damage and High- Versus Normal-Tension Glaucoma

The eyes with NTG were no more likely to have macular damage than were the eyes with HTG. In particular, 23.7% of the 38 eyes with normal tension had macular damage, compared to 39.3% of the 28 eyes with high tension. However, 8 of the 13 eyes with only one abnormal hemifield had NTG, while only 1 of the 7 with both hemifields affected had NTG. This difference is even more extreme if we assume, as argued above, that both hemifields of P7 and P13 were abnormal. With these two included in the Both group, 8 of the 11 eyes (72.7%) with one hemifield affected had NTG, and 8 of the 9 (88.9%) with both hemifields affected had HTG.

## DISCUSSION

The general purpose of this study was to better understand the nature of early glaucomatous damage of the macula, especially as it manifests in circumpapillary RNFL thickness plots. To restrict our study to early glaucoma, only eyes with a MD better than  $-6$  dB on the 24-2 VF test were included. In fact, all 20 eyes had a 24-2 MD better than  $-5$  dB. Further, to avoid false positives, we included only the 20 eyes that were abnormal on both the 10-2 VF test and RGC+ probability plots, as defined by the cluster criteria mentioned above. The results argue that early glaucomatous damage involves both shallow widespread and deep local thinning of the circumpapillary RNFL. In addition, they suggest that the model of macular damage needs further elaboration.

### Relatively Deep Local RNFL Damage

In 7 eyes, the circumpapillary RNFL contained a relatively local region with severe thinning of the RNFL. This thinning included the region that the model associates with the macula. We called these "deep local defects" of the macula. Six of these eyes (P1-P6) had upper 10-2 VF defects and 1 (P9) a lower 10-2 VF defect. The 6 with upper VF defects had marked RNFL thinning in the inferior macular region near the border of the temporal and inferior quadrants, which included the inferior region of the temporal quadrant and the temporal portion of the inferior quadrant. This is the region of the disc we have previously associated with arcuate-like defects within the macula.<sup>10-12</sup> The point of maximal thinning occurs in a relatively narrow range between approximately  $-38^\circ$  and  $-65^\circ$  using the reference system in Figure 3.<sup>10</sup> We have referred to this region as the macular vulnerability zone (MVZ).<sup>12</sup> The associated RGCs fall in the region within the purple borders in Figure 1. Figures 3 and 8 show the RNFL scans of three examples, P1, P2 and P4, of patients with maximum thinning in the MVZ. Notice that there is a near total thinning; a similar pattern was seen in P3, P5, and P6.

In the present study, only 1 eye, P9 (Fig. 6), showed an analogous lower VF defect, with a deep RNFL thinning maximal at the border of the temporal and superior quadrants (Figs. 6, 8). Consistent with the model, there was an arcuate defect that spanned both the 10-2 and 24-2 VFs and was farther from fixation than the local defects in the upper VF/lower retina seen in P1 to P6.

The presence of deep, local macular VF defects in early glaucoma has been well documented in previous studies<sup>2-5,9,10</sup> and associated with severe thinning of the circumpapillary RNFL.<sup>10</sup> Consistent with our findings, these defects are more prevalent in the upper macular VF, where they are closer to fixation and deeper than those in the lower macular VF.<sup>4,5,9,10,16,29</sup> The literature also suggests that these defects

are relatively more common in eyes with NTG.<sup>29-34</sup> In the present study, the sample (7 eyes) with only deep local defects was small, but the trend is in the same direction, 13.1% of the NTG eyes versus 7.1% of the HTG eyes.

### Relatively Shallow Widespread RNFL Damage

The results for the Both group supply the best evidence for relatively shallow and widespread RGC+ and RNFL damage of the macula. All 7 of these eyes showed widespread loss of 10-2 sensitivity, thinning of the macular RGC+ layer, and thinning of the RNFL throughout the region that the model associated with the macula. In addition, P7 from the Upper group and P13 from the Lower group probably represent milder versions of shallow widespread damage. The shallow widespread damage can include most, or all, of the disc as in P13 and P17 (Figs. 8D, 8F), or only the temporal half of the disc as seen in P18 (Fig. 8E). P14, P15, and P19 show a combination of shallow widespread RNFL thinning of the macular region of the disc combined with more localized deeper RNFL defects; the latter appeared as deep defects on the 24-2 TD.

Because miosis and cataracts can produce widespread loss in visual sensitivity across the VF, the prevalence and nature of widespread or diffuse VF damage have been debated.<sup>17,18</sup> In general, however, the literature indicates that widespread loss can occur.<sup>1,6,19-23</sup> For example, Henson et al.<sup>19</sup> argued that there is often a widespread component to early glaucomatous damage seen on 24-2 VFs, although this is subtle ( $\leq 2$  dB) and typically associated with deeper, more localized VF defects. Our evidence for widespread damage of the macula rests largely on OCT findings, which are relatively unaffected by miosis or cataracts. Interestingly, all but one of our patients with widespread macular damage had HTG, consistent with the old view that diffuse loss is more commonly seen in cases with high IOP.<sup>20,22,30</sup>

### Implications for the Model of Macular Damage

Our model in Figure 1 was proposed to describe glaucomatous damage of the macula. It is a model of healthy anatomy, as well as a model of the location of glaucomatous damage. In other words, it has anatomical assumptions about the map between the location of macular RGCs and locations at the disc, as well as assumptions about the relative vulnerability of different parts of the disc to glaucomatous damage. The present results support the anatomical assumptions. In general, the thinning of the circumpapillary RNFL associated with VF and RGC macular abnormalities occurred in the region predicted by the model. However, the assumptions about relative vulnerability of different regions of the disc need elaborating.

The schematic model in Figure 1 presents a simplified picture of regions that are more or less vulnerable to relatively local glaucomatous damage. First, concerning relatively local damage, the MVZ (approximately  $-38^\circ$  to  $-65^\circ$ ) is associated with the inferior portion of the macula, while the equivalent region ( $38^\circ$ - $65^\circ$ ) located at the border of the temporal and superior quadrants of the disc is largely associated with the regions of the retina lying outside the macula. In addition, the defects in the MVZ tend to be deeper, and probably more numerous as well. See our earlier studies<sup>11,12</sup> for a discussion of possible reasons for greater vulnerability of the MVZ.

In addition to local RNFL defects, many of the eyes with abnormal macular VFs and RGC+ maps showed what could be considered widespread damage. This damage included the macular region and, in some cases, was relatively mild. To extend the model, we assume that shallow widespread thinning of the disc is equally likely to appear in the inferior

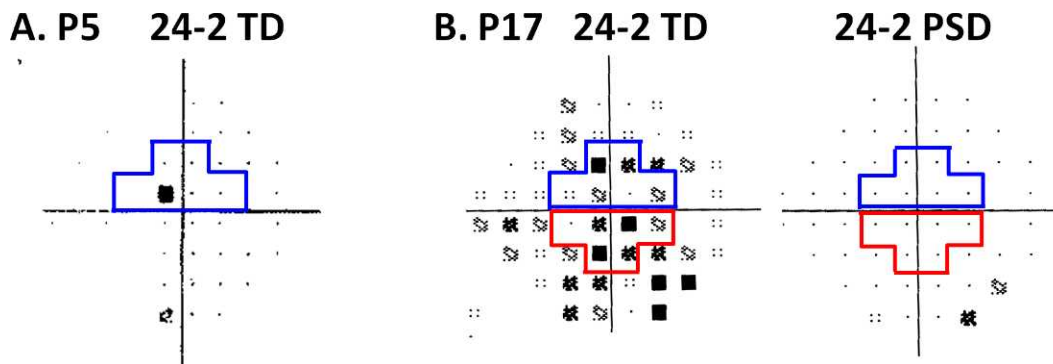


FIGURE 9. (A) The TD probability plot of P5's 24-2 VF. (B) The TD and PD probability plots of P17's 24-2 VF.

and superior macular region of the disc. Larger portions of the disc and, in some cases the entire disc, can be involved.

With the added assumptions about the nature of glaucomatous damage at the disc, the model explains a number of findings in the literature. First, as mentioned above, it has been reported that macular VF defects are more common in the upper VF, as well as more severe/deeper, and closer to fixation, as compared to defects in the lower VF.<sup>4,5,9,10,13,16,29</sup> According to the model, this is primarily due to the asymmetric wiring (Fig. 1) combined with the relatively more common and deeper RNFL defects in the MVZ compared to the equivalent location in the upper disc near the border of the temporal and superior quadrants. Second, the relative preponderance of upper versus lower VF defects will depend upon the test used, as well as the criteria for abnormality. With the 10-2 VF test and criteria favoring local and/or deep defects,<sup>9,10,16,29</sup> the relative number of upper VF defects will increase, while with the 24-2 VF test<sup>13</sup> and criteria favoring subtle defects,<sup>7,13</sup> the difference between the number of upper versus lower VF defects will decrease.

### Clinical Implications

Although the point has been made before, it is worth repeating here: Damage to the all-important macular region can be missed or underestimated with a VF test, like the 24-2, with a 6° test grid.<sup>8-13</sup> Twenty out of 66 eyes in this study had macular damage. Even deep local defects of the upper macular VF can be completely missed with the 24-2 VF test.<sup>10</sup> However, typically if damage is confined to the central 10°, it will appear as one or two abnormal central points on the 24-2 VFs,<sup>10</sup> as in the case of P5 (Fig. 9A). The 24-2 test pattern needs modification unless it is routinely used with a 10-2 test, which is often not the case.

Second, the subtle local VF defects associated with lower VF/superior macula, and/or widespread macular damage, may be overlooked or dismissed as insignificant based upon 24-2 VFs, especially if only PD plots are examined. The 24-2 VFs for P17 in Figure 9B provide an example. The pattern standard deviation (PSD; 1.62 dB) was in the normal range. Thus, macular damage can be missed if TD plots are ignored.

Third, the clinician is often faced with VFs that do not appear as typical or classic patterns.<sup>33,35</sup> In general, macular damage can present with a variety of patterns on the 24-2 and 10-2 VFs depending upon relative contributions of widespread and local defects, as well as the location of the local defects. The circumpapillary RNFL plot, if properly analyzed, can help the clinician understand VF patterns that appear unusual or ambiguous, as well as help identify macular damage.

Fourth, for identifying local damage to the macula, we find the presentation in Figure 3A particularly helpful and a careful scrutiny of the disc scan essential. The scan and RNFL plot are presented with the center of the temporal region of the disc in the center of the display, instead of the usual TSNIT arrangement, which is centered on the nasal quadrant. This NSTIN plot has the advantage of placing the important macular region in the center, rather than splitting it in half. (Note that the center of the temporal quadrant does not correspond to the midline of the VF [see Fig. 3C].) In the NSTIN format of Figure 3A, the macula is represented by the region between the red and blue lines in the center of the scan. It is also important that the scan itself be large enough that the clinician can scrutinize carefully the macular region, looking for local thinning and checking the veridicality of the segmentation of the RNFL, as all segmentation algorithms make mistakes. Figure 10 illustrates these points. This patient had a 24-2 VF test with a MD (−1.50 dB), a PSD (1.16 dB), and a glaucoma hemifield test (GHT) all within normal limits. While there were a few abnormal points on the 10-2 test, the 10-2 MD (−1.70 dB) and PSD (1.39 dB) were within normal limits (Fig. 10A). The RNFL profile produced by the machine (Fig. 10B) was also unremarkable. However, the algorithm appears to miss a thinning as indicated by the white arrow in Figure 10B, which is at a higher magnification than in the typical OCT report. Figure 10C shows an enlargement of this region with and without correction. After correcting the segmentation algorithm, the RNFL plot (Fig. 10D) shows a clear abnormal region (black arrow). In fact, this very local thinning is in the region associated with macular damage of the upper VF. An examination of the RGC+ thinning and probability plots confirms RGC+ damage as indicated by the arrows in Figure 10E. As further evidence that this damage is the source of the problem seen on the 10-2, the 10-2 results can be combined with RGC+ maps as previously suggested.<sup>28</sup> In Figure 10F, the abnormal points from the 10-2 PD plot in Figure 10A are superimposed on the RGC+ maps after adjusting for RGC displacement. The agreement confirms a local defect in the macula.

Finally, this study provides evidence that subtle thinning of the temporal quadrant can be missed on RNFL plots. For example, both P10 and P12 had clear RGC+ thinning in the inferior macula (Fig. 6), and the macular damage was confirmed with independent evidence—an intereye comparison of RNFL thickness in the case of P12 and an abnormal mfVEP in the case of P10. However, RNFL thickness in the temporal quadrant was in the normal range for both eyes. This is presumably due to the relatively thin RNFL in the temporal quadrant combined with the variability among healthy control eyes in this region. In any case, this argues for looking at RGC+

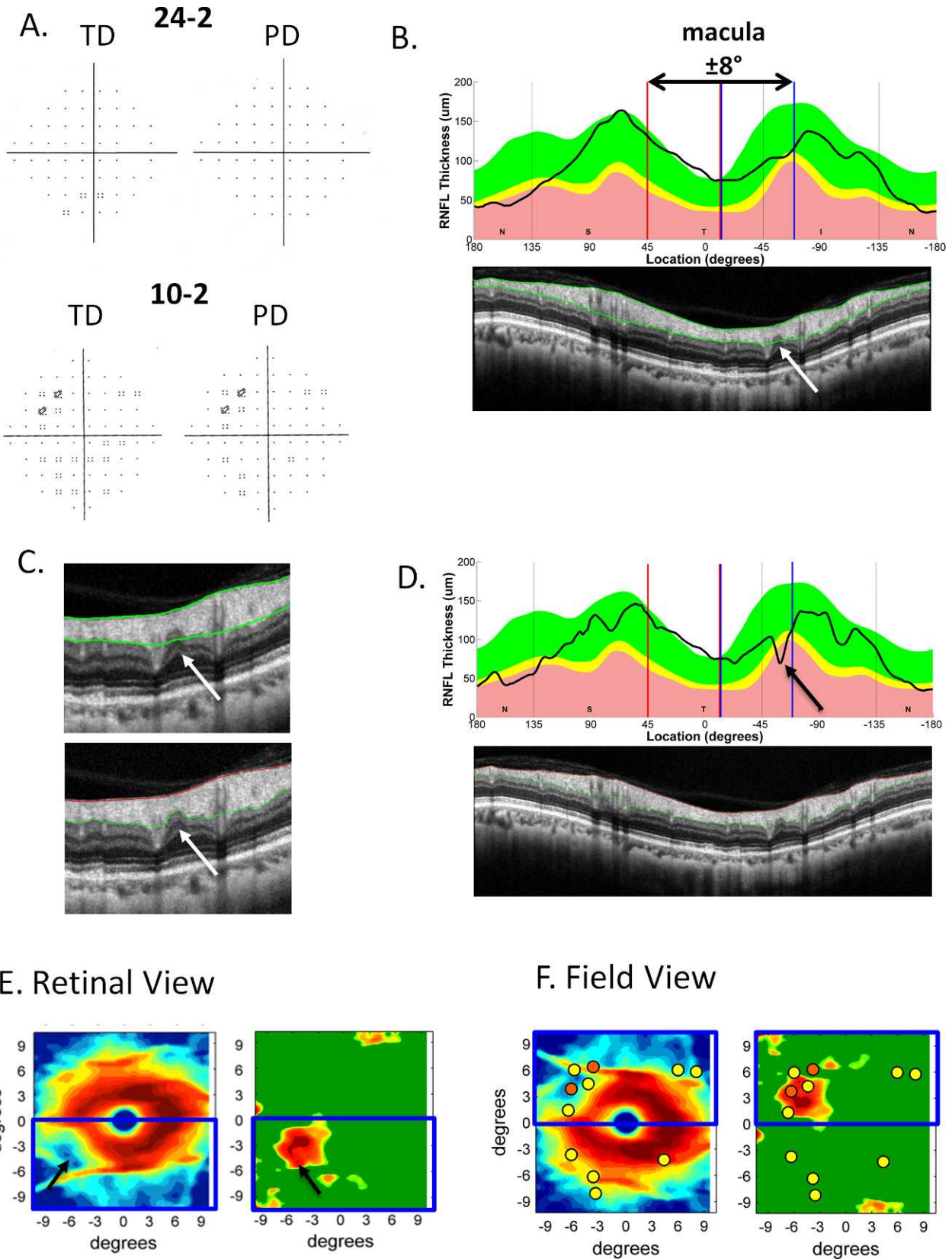


**FIGURE 10.** Optical coherence tomography and VF results from an eye of a glaucoma suspect. **(A)** The TD and PD probability plots for the 24-2 and 10-2 VF tests. **(B)** The RNFL thickness plot and circumpapillary scan as in Figure 3. **(C)** An expanded view of the region near the arrow in **(B)** with and without the segmentation corrected. **(D)** Same as in **(B)**, but with the automated segmentation corrected. **(E)** The RGC+ thickness and probability maps in retinal view. **(F)** The RGC+ thickness and probability maps in field view with the abnormal points from the 10-2 PD plot in **(A)** superimposed. Pseudocolor calibration bars are shown at the bottom of Figure 5.

maps, in addition to RNFL plots, when evaluating fdOCT scans for glaucomatous damage. We find the RGC+ probability plots most useful when combined with 10-2 VF data in a single plot as previously described<sup>28</sup> and illustrated in Figure 10F.

### Limitations

First, the number of eyes with macular damage, 20, is a relatively small sample; thus the details of the findings here will need replicating with a larger group. This is especially true for comparisons within the group of 20 eyes, such as the observed differences between patients with NTG versus HTG. Further, whenever a study excludes eyes, a selection bias is possible. Here we included only eyes with GON as seen on fundus photos. While one could argue that this resulted in a bias toward selecting for structural as opposed to functional changes, it should not have introduced a bias for detecting macula abnormalities, the focus of this study. On the other hand, if instead of using GON, we had studied only eyes with OHT, the proportion of eyes with abnormal 10-2 VFs and RGC thickness plots would have been lower, and the proportion with normal 10-2 VFs and RGC thickness would have been higher. Another obvious source of selection bias is the population seen by the referring ophthalmologists. The patients come to a tertiary practice where relatively more NTG suspects are referred because of the difficulty in diagnosing glaucoma when pressures are statistically low.

### Summary

Early glaucomatous damage to the macula is due to widespread and/or local circumpapillary RNFL defects. The local macular damage is more common, more severe, and closer to fixation in the upper VF/inferior retina than in the lower VF/superior retina. A model of glaucomatous damage of the macula predicts the location of both the widespread and local defects. Optical coherence tomography scans of the circumpapillary RNFL and the macular RGC+ layer can aid in the identification of these defects and help in the interpretation of 24-2 and 10-2 VF tests.

### Acknowledgments

The authors thank Diane Wang and David Rhee for help with the figures; Monica Chen, Alyssa Ehrlich, and Diane Wang for comments on the manuscript; and Jeffrey Liebmann and Celso Tello for referring patients for the study.

Supported by National Institutes of Health Grant R01-EY02115 (DCH) and a grant from Topcon Corp.

Disclosure: **D.C. Hood**, Topcon Corp. (F, C); **A. Slobodnick**, None; **A.S. Raza**, None; **C.G. de Moraes**, None; **C.C. Teng**, None; **R. Ritch**, None

### References

- Curcio CA, Allen KA. Topography of ganglion cells in human retina. *J Comp Neurol*. 1990;300:5-25.
- Aulhorn E, Harms M. Early visual field defects in glaucoma. In: Leydhecker W, ed. *Glaucoma, Tutzing Symposium*. Basel: Karger; 1967:151-156.
- Drance SM. The early field defects in glaucoma. *Invest Ophthalmol*. 1969;8:84-91.
- Aulhorn E, Karmeyer H. Frequency distribution in early glaucomatous visual field defects. *Doc Ophthalmol Proc Ser*. 1977;14:75-83.
- Nicholas SP, Werner EB. Location of early glaucomatous visual field defects. *Can J Ophthalmol*. 1980;15:131-133.

- Anctil JL, Anderson DR. Early foveal involvement and generalized depression of the visual field in glaucoma. *Arch Ophthalmol*. 1984;102:363-370.
- Heijl A, Lundqvist L. The frequency distribution of earliest glaucomatous visual field defects documented by automatic perimetry. *Acta Ophthalmol (Copenh)*. 1984;62:658-664.
- Langerhorst CT, Carenini LL, Bakker D, De Bie-Raakman MAC. Measurements for description of very early glaucomatous field defects. In: Wall M, Heijl A, eds. *Perimetry Update 1996/1997*. New York: Kugler Publications; 1997:67-73.
- Schiefer U, Papageorgiou E, Sample PA, et al. Spatial pattern of glaucomatous visual field loss obtained with regionally condensed stimulus arrangements. *Invest Ophthalmol Vis Sci*. 2010;51:5685-5689.
- Hood DC, Raza AS, de Moraes CG, et al. Initial arcuate defects within the central 10 degrees in glaucoma. *Invest Ophthalmol Vis Sci*. 2011;52:940-946.
- Hood DC, Raza AS, de Moraes CG, Johnson CA, Liebmann JM, Ritch R. The nature of macular damage in glaucoma as revealed by averaging optical coherence tomography data. *Trans Vis Sci Technol*. 2012;1:1-15.
- Hood DC, Raza AS, de Moraes CG, Liebmann JM, Ritch R. Glaucomatous damage of the macula. *Prog Retin Eye Res*. 2013;32:1-21.
- Traynis I, de Moraes CG, Raza AS, Liebmann JM, Ritch R, Hood DC. The prevalence and nature of early glaucomatous defects in the central 10° of the visual field. *JAMA Ophthalmol*. In press.
- Garway-Heath DE, Poinoosawmy D, Fitzke FW, Hitchings RA. Mapping the visual field to the optic disc in normal tension glaucoma eyes. *Ophthalmology*. 2000;107:1809-1815.
- Hood DC, Anderson S, Rouleau J, et al. Retinal nerve fiber structure versus visual field function in patients with ischemic optic neuropathy: a test of a linear model. *Ophthalmology*. 2008;115:90-101.
- Su D, Park SC, Simonson JL, et al. Progression pattern of initial parafoveal scotomas in glaucoma. *Ophthalmology*. 2013;120:520-527.
- Heijl A. Lack of diffuse loss of differential light sensitivity in early glaucoma. *Acta Ophthalmol*. 1989;67:353-360.
- Åsman P, Heijl A. Diffuse visual field loss and glaucoma. *Acta Ophthalmol*. 1994;72:303-308.
- Henson DB, Artes PH, Chauhan BC. Diffuse loss of sensitivity in early glaucoma. *Invest Ophthalmol Vis Sci*. 1999;40:3147-3151.
- Drance SM, Douglas GR, Airaksinen PJ, et al. Diffuse visual field loss in chronic open-angle glaucoma and low-tension glaucoma. *Am J Ophthalmol*. 1987;104:577-580.
- Drance SM. Diffuse visual field loss in open-angle glaucoma. *Ophthalmology*. 1991;98:1533-1538.
- Caprioli J, Sears M, Miller JM. Patterns of early visual field loss in open-angle glaucoma. *Am J Ophthalmol*. 1987;103:512-517.
- Artes PH, Chauhan BC, Keltner JL, et al.; Ocular Hypertension Treatment Study Group. Longitudinal and cross-sectional analyses of visual field progression in participants of the Ocular Hypertension Treatment Study. *Arch Ophthalmol*. 2010;128:1528-1532.
- Wong WL, Li X, Jialiang L, et al. Cataract conversion assessment using Lens Opacity Classification System III and Wisconsin Cataract Grading System. *Invest Ophthalmol Vis Sci*. 2013;54:280-287.
- Richter BA, Chung J, Azen SP, et al. Prevalence of visually significant cataract and factors associated with unmet need for cataract surgery: Los Angeles Latino Eye Study. *Ophthalmology*. 2009;116:2327-2335.

26. Yang Q, Reisman CA, Wang Z, et al. Automated layer segmentation of macular OCT images using dual-scale gradient information. *Opt Express*. 2010;18:21293-21307.
27. Raza AS, Cho JS, de Moraes CGV, et al. Retinal ganglion cell layer thickness and local visual field sensitivity in glaucoma. *Arch Ophthalmol*. 2011;129:1529-1536.
28. Hood DC, Raza AS. Method for comparing visual field defects to local RNFL and RGC damage seen on frequency domain OCT in patients with glaucoma. *Biomed Opt Express*. 2011;2:1097-1105.
29. Park SC, De Moraes CG, Teng CC, Tello C, Liebmann JM, Ritch R. Initial parafoveal versus peripheral scotomas in glaucoma: risk factors and visual field characteristics. *Ophthalmology*. 2011;118:1782-1789.
30. Chauhan BC, Drance SM, Douglas GR, et al. Visual field damage in normal-tension and high-tension glaucoma. *Am J Ophthalmol*. 1989;108:636-642.
31. Hitchings RA, Anderton SA. A comparative study of visual field defects seen in patients with low tension glaucoma and chronic simple glaucoma. *Br J Ophthalmol*. 1983;67:818-821.
32. Caprioli J, Spaeth GL. Comparison of visual field defects in the low-tension glaucoma with those in the high-tension glaucoma. *Am J Ophthalmol*. 1984;97:730-737.
33. Zeiter JH, Shin DH, Juzych MS, et al. Visual field defects in patients with normal-tension glaucoma and patients with high-tension glaucoma. *Am J Ophthalmol*. 1992;114:758-763.
34. Thonginnetra O, Greenstein VC, Chu D, et al. Normal versus high tension glaucoma: a comparison of functional and structural deficits. *J Glaucoma*. 2010;19:151-157.
35. Keltner JL, Johnson CA, Cello KE, et al.; Ocular Hypertension Treatment Study Group. Classification of visual field abnormalities in the ocular hypertension treatment study [erratum published in *Arch Ophthalmol*. 2008;126:561]. *Arch Ophthalmol*. 2003;121:643-650.